Applied Physics A (2021) 127:429
https://doi.org/10.1007/s00339-021-04551-4

Applied Physics A
Materials Science & Processing

Phonon frequencies, mechanical and optoelectronic properties for $InP_xAs_ySb_{1-x-y}$/InAs alloys under the influence of pressure

A. R. Degheidy[1] · A. M. AbuAli[2] · Elkenany. B. Elkenany[1]

Received: 5 January 2021 / Accepted: 21 April 2021 / Published online: 18 May 2021

Abstract

The pressure dependence of electronic and optical properties for $InP_xAs_ySb_{1-x-y}$ alloys lattice matched to InAs substrate has been investigated. The mechanical properties and the phonon frequencies for $InP_xAs_ySb_{1-x-y}$/InAs system under the effect of pressure have been studied. The physical properties of the binary components InP, InAs and InSb that constitute the quaternary alloy were used in this analysis. The study achieved using the empirical pseudo-potential approach (EPM) under the virtual crystal approximation (VCA). Our findings were found to be in good agreement with experimental and theoretical data at $p=0$ kbar. Our results may serve as reference for the future experimental values at high pressures. The pressure dependence of the fundamental properties of $InP_xAs_ySb_{1-x-y}$/InAs system such as optical constants and modes of lattice vibration has not been fully studied. So, we have concentrated on these properties under the effect of pressure.

Keywords Phonon frequencies · Mechanical properties · Optoelectronic properties · Alloys · Pressure

1 Introduction

The III–V semiconductors are major materials used in manufacturing high-speed electronics, long-wavelength devices [1–5]. In the recent years, the ternary and quaternary compounds of the III–V groups have been the subject to several experimental and hypothetical analysis [6–9]. The binary compounds InP, InAs and InSb form continuous series of alloys denoted by $InP_xAs_ySb_{1-x-y}$ over the entire range of the composition parameters of x and y. The study of such quaternary alloys is making use of the data available for the binary compounds which constitute them. It has many applications as a source and detector of long-wavelength light communication systems. The recent usage of such alloy is designing low-loss optical fibers in the 2–4 μm wavelength region [10–14]. $InP_xAs_ySb_{1-x-y}$ lattice matched to InAs is also used to build low-temperature TPV cells (thermo-photovoltaic cells) in the range of 0.35–0.5 eV [15]. It is important to examine the electrical, optical, mechanical and thermal properties of semiconductor compounds, as this regulates us in the planning of high-performance electronic devices [13, 16–23]. The $InP_xAs_ySb_{1-x-y}$ quaternary structure has an important role in the electronic applications. So, we have studied thoroughly its basic properties such as electronic, optical properties and lattice vibration modes and their dependence on pressure. The quaternary $InP_xAs_ySb_{1-x-y}$ alloy can be lattice matched to two different substrates, InAs and GaSb, and in this work, we used InAs substrate.

The EPM is one of several techniques for determining the band structure of semiconductor materials [16, 24]. Many studies have been done on the effects of pressure and temperature on the physical properties of materials [24–29]. Sadao Adachi [10] studied the band gaps and refractive indices of InPAsSb, GaInAsSb and AlGaAsSb. To the best of our knowledge, the optical, electronic, mechanical and vibrational properties in $InP_xAs_ySb_{1-x-y}$/InAs system under the effect of pressure have not been fully studied so far.

In the present work, the pressure dependence of optoelectronic and vibrational properties for the quaternary alloy $InP_xAs_ySb_{1-x-y}$ lattice matched to InAs was studied. Our calculations were based on the empirical pseudo-potential method (EPM) [30–32] with the virtual crystal approximation (VCA) [33, 34].

✉ Elkenany. B. Elkenany
kena@mans.edu.eg

[1] Department of Physics, Faculty of Science, Mansoura University, P. O. Box: 35516, Mansoura, Egypt

[2] Zewail City of Science and Technology, University of Science and Technology, P. O. Box: 12578, October City, Giza, Egypt

2 Computational method

The calculations were performed using essentially the (EPM) under the (VCA). Based on this method, one can deduce the pseudo-potential form factors of $InP_xAs_ySb_{1-x-y}$ lattice matched to InAs substrate at zero pressure. The lattice matching condition is given by $x = ay + b$, where x and y are the compositional parameters as reported by Adachi [11], where:

$$a = \frac{a_{\mathrm{InAs}} - a_{\mathrm{InSb}}}{a_{\mathrm{InP}} - a_{\mathrm{InSb}}} \tag{1}$$

$$b = \frac{a_{\mathrm{Substrate}} - a_{\mathrm{InSb}}}{a_{\mathrm{InP}} - a_{\mathrm{InSb}}} \tag{2}$$

It was found that the lattice matching condition for InAs substrate between x and y:

$$x = 0.68933 - 0.68933y \tag{3}$$

The energy eigenvalues of the binary compounds which constitute the quaternary alloy could be determined by solving the secular determinant in numerical techniques [35–37].

$$\left\| \left(\frac{1}{2}\left|\mathbf{k} + \mathbf{G}'\right|^2 - \mathrm{E}_{n\mathbf{k}} \right) \delta_{\mathbf{G}\,\mathbf{G}'} + \sum_{\mathbf{G}\neq\mathbf{G}}{}' V(|\Delta\mathbf{G}|) \right\| = 0 \tag{4}$$

where **G** and **k** are the reciprocal lattice vector and the wave vector, respectively. The electronic energy band gaps could be calculated from the obtained energy eigenvalues. More details about this method stated in Refs. [35–37]. The form factors have been obtained by fitting the band gap energies of AlP and AlSb at the high symmetric points $L(0.5,0.5,0.5)$, $\Gamma(0,0,0)$ and $X(0,0,1)$ in the Brillouin zone to the experimental values. The dimension of our eigen-value problem is a (65×65) matrix which provides generally good convergence. The pseudo-potential form factors and the lattice constant for the quaternary alloy could be determined as follow [11]:

$$W(x,y) = xW_{\mathrm{InP}} + yW_{\mathrm{InAs}} + (1-x-y)W_{\mathrm{InSb}} \tag{5}$$

$$a(x,y) = xa_{\mathrm{InP}} + ya_{\mathrm{InAs}} + (1-x-y)a_{\mathrm{InSb}} \tag{6}$$

The calculated direct n and indirect energy band gaps of $InP_xAs_ySb_{1-x-y}$/InAs system are shown in Table 1. It should be mentioned that the pressure range in our calculations was performed through the stability of the crystal structure. As a matter of fact, in the pressure range 0–120 kbar, the structure of the material under investigation was still zinc blende. The polarity α_p of the alloys of interest could be determined by using Vogl's relation [38]. The elastic constants (c_{11}, c_{12}, c_{44}) and elastic moduli (bulkB_u, shear C_s, young Y_o) could be investigated according to Refs.[30, 39–42]. By knowing the fundamental energy band gap, the calculations of optical properties could be determined as refractive index, high frequency dielectric constant ε_∞ and static dielectric constant ε_s. The longitudinal and transverse phonon frequencies $\omega_{\mathrm{LO}}, \omega_{\mathrm{TO}}$ could be determined by solving the Lyddane–Sachs–Teller relations [43, 44].

$$\frac{\omega_{\mathrm{TO}}^2}{\omega_{\mathrm{LO}}^2} = \frac{\varepsilon_\infty}{\varepsilon_s} \tag{7}$$

$$\omega_{\mathrm{LO}}^2 - \omega_{\mathrm{TO}}^2 = \frac{4\pi\left(e_T^*\right)^2 e^2}{M\Omega_o\varepsilon_\infty} \tag{8}$$

where ε_∞,ε_s M and Ω_0 are the optical dielectric constant, static dielectric constant, twice of reduced mass and the volume occupied by one atom, respectively. The calculations of $InP_xAs_ySb_{1-x-y}$ alloys are done using our own code based on MATLAB language.

3 Results and discussions

Table 1 and Fig. 1 show the effect of pressure from 0 to 120 kbar on the energy gaps of $InP_xAs_ySb_{1-x-y}$ lattice matched to InAs substrate for different compositional parameter y. It can be noticed that the energy gaps are increased at the Γ, L high symmetry points and decreased at X-point when the pressure increases. Due to this behavior, the quaternary alloy converts from a direct band gap semiconductor to an

Table 1 Energy gaps of $InP_xAs_ySb_{1-x-y}$/InAs at different values of pressure at constant values of compositional parameter

	$y=0$			$y=0.5$			$y=1$ (InAs)		
P(kbar)	E_L(eV)	E_Γ (eV)	E_X(eV)	E_L(eV)	E_Γ (eV)	E_X(eV)	E_L(eV)	E_Γ (eV)	E_X(eV)
0	1.597	1.012	2.056	1.329	0.655	1.761	1.049, 1.07[a]	0.359, 0.360[a]	1.495, 1.37[a]
30	1.765	1.285	1.929	1.509	0.963	1.632	1.244	0.701	1.365
60	1.922	1.542	1.8	1.677	1.252	1.5	1.425	1.023	1.23
90	2.068	1.782	1.67	1.832	1.524	1.366	1.591	1.327	1.092
120	2.203	2.008	1.539	1.974	1.779	1.23	1.742	1.613	0.95

[a]Ref [46]

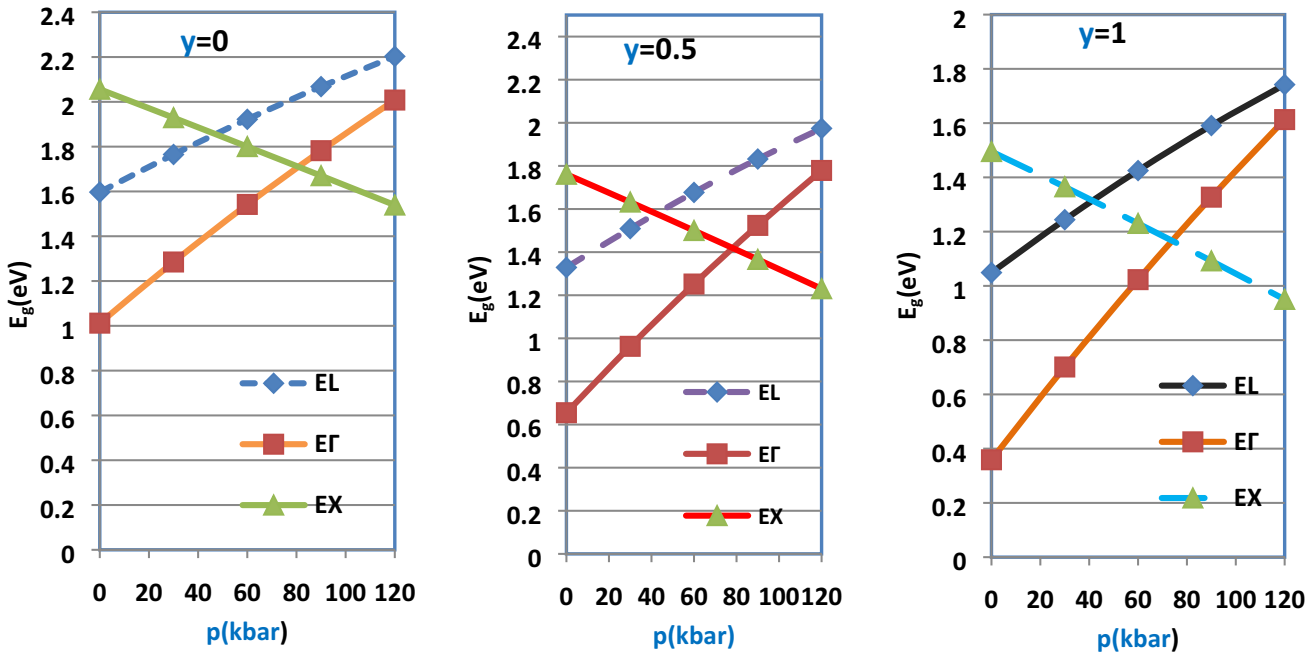

Fig. 1 The energy gaps of $InP_xAs_ySb_{1-x-y}$/InAs as function of pressure at different values of y-composition parameter (0, 0.5, 1)

indirect one at a certain threshold value of pressure for every composition value. These inversion points were found to be ($y=0$, $p=81$ kbar), ($y=0.5$, $p=78.5$ kbar) and ($y=1$, $p=74$ kbar). The energy band gaps of $InP_xAs_ySb_{1-x-y}$/InAs as function of pressure were fitted by polynomials to give.

At y = 0

$$E_L(p) = 1.597 + 0.0058p - 6\times10^{-6}p^2 \quad (9)$$

$$E_\Gamma(p) = 1.012 + 0.0094p - 9\times10^{-6}p^2 \quad (10)$$

$$E_X(p) = 2.056 - 0.0042p - 7\times10^{-7}p^2 \quad (11)$$

At y = 0.5

$$E_L(p) = 1.329 + 0.0062p - 7\times10^{-6}p^2 \quad (12)$$

$$E_\Gamma(p) = 0.655 + 0.0105p - 1\times10^{-5}p^2 \quad (13)$$

$$E_X(p) = 1.761 - 0.0043p - 1\times10^{-6}p^2 \quad (14)$$

At y = 1

$$E_L(p) = 1.049 + 0.0068p - 8\times10^{-6}p^2 \quad (15)$$

$$E_\Gamma(p) = 0.359 + 0.0117p - 1\times10^{-5}p^2 \quad (16)$$

$$E_X(p) = 1.495 - 0.0043p - 2\times10^{-6}p^2 \quad (17)$$

Eqs. (9–17) can be used to predict the energy band gaps for the considered alloy for different pressures. Our calculated data at ($y=1$ (InAs) & $p=0$ kbar) of the E_L, E_Γ and E_X are in excellent agreement with the published values of 1.07 eV [45, 46], 0.36 eV [45, 46] and 1.37 eV [45, 46], respectively. Our calculated results of the energy band gaps for the $InP_xAs_ySb_{1-x-y}$/InAs system at high pressures may serve as reference for the experimental work.

The electronic band structure has been determined by using the (EPM) with including (VCA). Figure 2a shows the crystal structure for $InP_xAs_ySb_{1-x-y}$ alloy which has a face-centered cubic (FCC) lattice structure. The quaternary $InP_xAs_ySb_{1-x-y}$ alloy consists from four elements (In, P, As and Sb) or from three binary materials (InP, InAs and InSb). The electronic band structure of states for $InP_xAs_ySb_{1-x-y}$ /InAs system for $p=0$ kbar (solid lines) and $p=120$ kbar (dashed lines) for composition $y=0.5$ is displayed in Fig. 2b. It is observed from Fig. 2b that with increasing pressure, the minima of the conduction band at (Γ, L) points go up and at X-point go down. Consequently, the band gap at the Γ, L points increases, while at X-point decreases. It is seen that the conduction energy bands are more influenced by pressure than the valence energy bands. These properties of the alloy under investigation are desirable for the optoelectronic applications.

The elastic constants are significant parameters that characterize the reaction to the macroscopic applied stress.

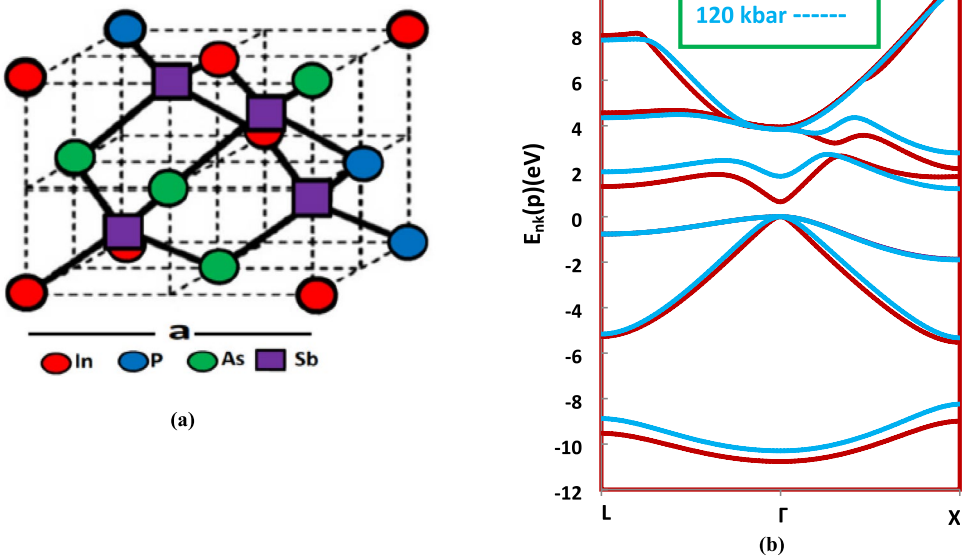

Fig. 2 The crystal structure (**a**) and electronic band structure for $InP_xAs_ySb_{1-x-y}$/InAs system for $p=0$ kbar (solid lines) and $p=120$ kbar (dashed lines) for composition y = 0.5 (**b**)

The elastic constants C_{11}, C_{12} and C_{44} for the zinc blende $InP_xAs_ySb_{1-x-y}$/InAs system are listed in Table 2. Figure 3 displays the dependence of elastic constants (10^{12}dyn/cm^2) on pressure for different constant values of y (0, 0.5, 1). It is noticed that all the elastic constants are increased with increasing pressure. The C_{11} exhibits the largest values as compared to C_{12} and C_{44} and more affected by the pressure than C_{12} and C_{44}. The calculated elastic constants are fitted by polynomials in 10^{12} dyne cm^{-2} that give the following relations:

At $y=0$

$$C_{11}(p) = 0.905 + 0.0004p - 5\times10^{-8}p^2 \quad (18)$$

$$C_{12}(p) = 0.391 + 0.0002p - 5\times10^{-8}p^2 \quad (19)$$

$$C_{44}(p) = 0.365 + 0.0002p - 1\times10^{-7}p^2 \quad (20)$$

At $y=0.5$

$$C_{11}(p) = 0.918 + 0.0004p - 2\times10^{-7}p^2 \quad (21)$$

$$C_{12}(p) = 0.396 + 0.0002p - 2\times10^{-7}p^2 \quad (22)$$

$$C_{44}(p) = 0.371 + 0.0002p + 9\times10^{-8}p^2 \quad (23)$$

At $y=1$

$$C_{11}(p) = 0.931 + 0.0005p - 1\times10^{-7}p^2 \quad (24)$$

$$C_{12}(p) = 0.402 + 0.0002p - 9\times10^{-8}p^2 \quad (25)$$

$$C_{44}(p) = 0.376 + 0.0002p - 9\times10^{-8}p^2 \quad (26)$$

Eqs. (18–26) can be used to predict the elastic constants for the $InP_xAs_ySb_{1-x-y}$/InAs system for different values of pressure. Our calculated values at ($y=1$ & $p=0$ kbar) of the C_{11}, C_{12} and C_{44} are in excellent accord with the published data of ($0.943*10^{12}$ dyn/cm^2) [47], ($0.407*10^{12}$

Table 2 The elastic constants (10^{12} dyn/cm^2) of $InP_xAs_ySb_{1-x-y}$/InAs system for various pressures for different values of compositional parameter y

	y = 0			$y=0.5$			$y=1$ (InAs)		
P(kbar)	c_{11}	c_{12}	c_{44}	c_{11}	c_{12}	c_{44}	c_{11}	c_{12}	c_{44}
0	0.905	0.391	0.365	0.918	0.396	0.371	0.931, 0.943[a]	0.402, 0.407[a]	0.376, 0.3819[a]
30	0.916	0.396	0.37	0.931	0.402	0.376	0.945	0.408	0.382
60	0.928	0.4	0.375	0.944	0.407	0.381	0.959	0.413	0.388
90	0.939	0.405	0.38	0.956	0.412	0.387	0.973	0.419	0.393
120	0.95	0.41	0.384	0.968	0.417	0.392	0.986	0.424	0.399

[a]Ref [47]

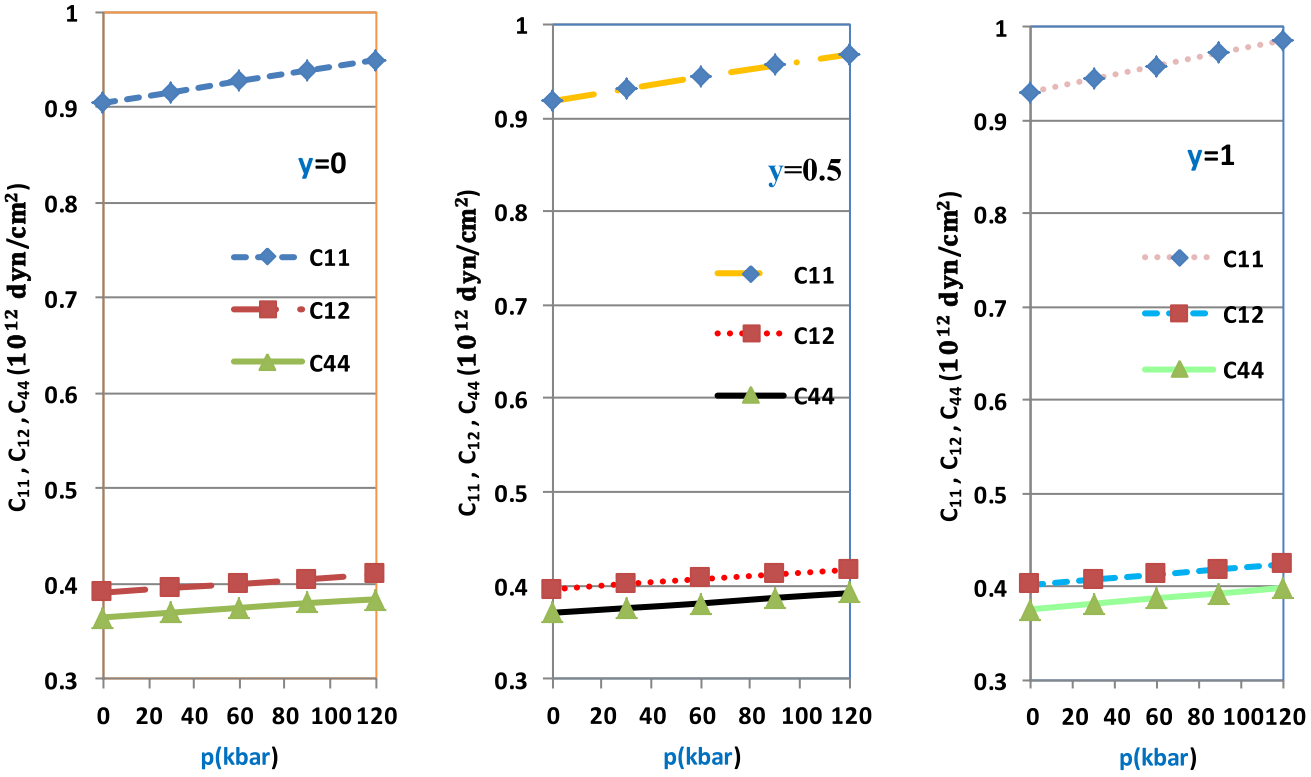

Fig. 3 The elastic constants (10^{12} dyn/cm^2) of $InP_xAs_ySb_{1-x-y}$/InAs as function of pressure for different values of compositional parameter y

dyn/cm^2) [47] and (0.3819*10^{12} dyn/cm^2) [47], respectively. Our calculated data of the elastic constants for the $InP_xAs_ySb_{1-x-y}$/InAs system at high pressures may serve as reference for the future experimental values.

Table 3 and Fig. 4 show the elastic moduli (B_u,C_s,Y_o) of $InP_xAs_ySb_{1-x-y}$ /InAs system under the effect of pressure for different values of compositional parameter y (0, 0.5 and 1). It can be noticed that all the mechanical moduli are increased with enhancing pressure. It is seen from Table 3 that the B_u/C_s ratio is greater than 1.75 which is the critical value that separates ductile and brittle materials [48]. The high values are associated with the ductility, whereas the low values correspond to the brittle nature. The calculated B_u/C_s values of $InP_xAs_ySb_{1-x-y}$ are greater than 1.75 for all values of pressure and for $y=0$, 0.5 and 1. So, this alloy is classified as a ductile material over the whole range of pressure. There is an excellent agreement between our calculated values and the available published ones [46, 48, 49].

In the design and manufacturing of electronic devices such as photonic crystals, wave guides, solar cells and detectors, the refractive index and optical dielectric constants are important parameters. Table 4 and Fig. 5 display the effect of pressure on the refractive index n, the static dielectric constant ε_0 and the high frequency dielectric constant ε_∞ of $InP_xAs_ySb_{1-x-y}$ lattice matched to InAs substrate for different values of composition y (0, 0.5 and 1). It will be noted that the refractive index n, the static dielectric constant ε_0 and the high frequency dielectric constant ε_∞ are decreased with increasing pressure. Also, it can be seen that the refractive index n, the static dielectric constant ε_0 and the high frequency dielectric constant ε_∞ are increased with increasing the composition from 0 to 1. There is an excellent agreement between our calculated values and experimental ones [43, 45, 50–52].

By solving the Lyddane–Sachs–Teller relationships, the longitudinal and the transversal optical phonon frequencies (ω_{LO}, ω_{TO}) of $InP_xAs_ySb_{1-x-y}$/InAs system could be determined [43, 44]. Our calculated results are listed in Table 5 and illustrated in Fig. 6 which shows the dependence of the phonon frequencies on pressure at different compositions y (0, 0.5 and 1). Both ω_{LO} and ω_{TO} are increased by increasing pressure, and however, the separations between them are slightly affected with pressure. It is observed from this figure that the values of ω_{LO} and ω_{TO} are shifted downward when the concentration is increased along the range (0–1). On the other words, the ω_{LO} and ω_{TO} are decreased with enhancing composition. The following polynomials show the best fits of their pressure dependence.

At $y=0$

Table 3 The elastic moduli (10^{12}dyn/cm^2) of $InP_xAs_ySb_{1-x-y}$/InAs at different values of pressure at constant values of compositional parameter y

	$y=0$				$y=0.5$				$y=1$ (InAs)			
P(kbar)	B_u	C_s	B_u/C_s	Y_0	B_u	C_s	B_u/C_s	Y_0	B_u	C_s	B_u/C_s	Y_0
0	0.562	0.2568	2.1885	0.669	0.57	0.2608	2.1856	0.679	0.578, 0.579[b]	0.2647, 0.268[c]	2.1836	0.689, 0.698[a]
30	0.569	0.2603	2.1859	0.678	0.578	0.2646	2.1844	0.689	0.587	0.2689	2.1830	0.7
60	0.576	0.2637	2.1843	0.686	0.586	0.2684	2.1833	0.699	0.595	0.273	2.1795	0.71
90	0.583	0.2671	2.1827	0.695	0.593	0.2721	2.1793	0.708	0.603	0.277	2.1769	0.721
120	0.59	0.2704	2.1820	0.704	0.601	0.2757	2.1799	0.717	0.611	0.2808	2.1759	0.731

[a]Ref. [47], [b]Ref. [49], [c]Ref [46]

$$\omega_{LO}(p) = 5.623 + 0.0161p + 1\times10^{-5}p^2 \quad (27)$$

$$\omega_{TO}(p) = 5.278 + 0.0163p + 1\times10^{-5}p^2 \quad (28)$$

At $y=0.5$

$$\omega_{LO}(p) = 4.9591 + 0.0172p + 2\times10^{-5}p^2 \quad (29)$$

$$\omega_{TO}(p) = 4.6825 + 0.0174p + 3\times10^{-5}p^2 \quad (30)$$

At $y=1$

$$\omega_{LO}(p) = 4.4597 + 0.0183p + 4\times10^{-5}p^2 \quad (31)$$

$$\omega_{TO}(p) = 4.2362 + 0.0185p + 4\times10^{-5}p^2 \quad (32)$$

The expressions (27–32) can be used to predict the phonon frequencies ω_{LO} and ω_{TO} for the alloys under investigation for various pressures. Our calculated results at ($y=1$ (InAs) & $p=0$ kbar) of the LO(Γ) and TO(Γ) modes are in good agreement with the experimental values of ($4.5*10^{13}$ s^{-1}) [43], ($4.1*10^{13}$ s^{-1}) [43] and theoretical values of ($5.2*10^{13}$ s^{-1}) [45], ($4.9*10^{13}$ s^{-1}) [45], respectively. The calculated values of ω_{LO} and ω_{TO} at high values of pressure may serve as reference for the experimental work.

4 Conclusions

In this paper, we have presented a study of electronic structure, elastic constants and the related mechanical properties for $InP_xAs_ySb_{1-x-y}$ lattice matched to InAs in the zinc-blende structure using the empirical pseudopotential approach under the virtual crystal approximation. The pressure dependence of the optical properties as refractive index, high frequency and static dielectric constants has been determined. The longitudinal and transverse phonon frequencies of the alloys of interest are also examined. All studied quantities are studied under pressure up to 120 kbar. Our calculated values of the optical, electronic, mechanical properties and phonons frequencies for the considered alloys are found to be in a reasonable agreement with the experimental values. The calculated results in the present work seem likely to be useful as reference to the quantities that are not easily experimentally

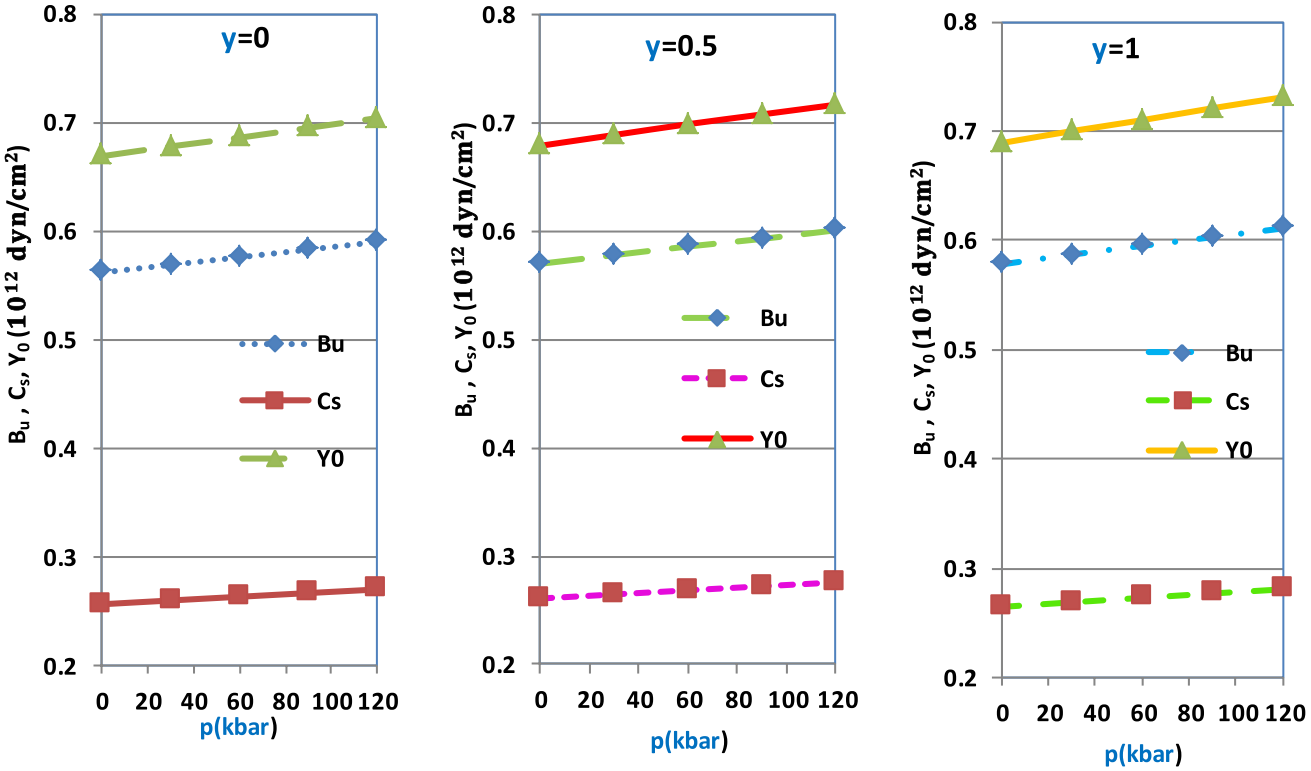

Fig. 4 The mechanical moduli s (10^{12} dyn/cm^2) of $InP_xAs_ySb_{1-x-y}$/InAs as function of pressure for different values of compositional parameter y (0, 0.5, 1)

Table 4 The refractive index, optical dielectric constant and static dielectric constant of $InP_xAs_ySb_{1-x-y}$/InAs at different values of pressure at constant values of compositional parameter *y*

	y=0			*y*=0.5			*y*=1		
P(kbar)	*n*	ε_∞	ε_s	*n*	ε_∞	ε_s	*n*	ε_∞	ε_s
0	3.241	10.5	11.92	3.5	12.25	13.74	3.754, 3.75[a], 3.51[b]	14.09, 14.08[c], 12.3[d]	15.62, 15.15[a], 15.42[c]
30	3.07	9.43	10.56	3.274	10.72	11.85	3.464	12	13.1
60	2.928	8.57	9.49	3.09	9.55	10.42	3.233	10.45	11.25
90	2.808	7.89	8.62	2.937	8.63	9.3	3.046	9.28	9.85
120	2.706	7.32	7.92	2.81	7.89	8.4	2.892	8.36	8.77

[a]Ref. [51], [b]Ref. [50], [c]Ref. [45], [d]Ref. [43]

obtained, especially at high pressure. The electronic, optical and mechanical properties of the $InP_xAs_ySb_{1-x-y}$/InAs system make it a successful candidate for optoelectronic applications such as thermo-photovoltaic cells.

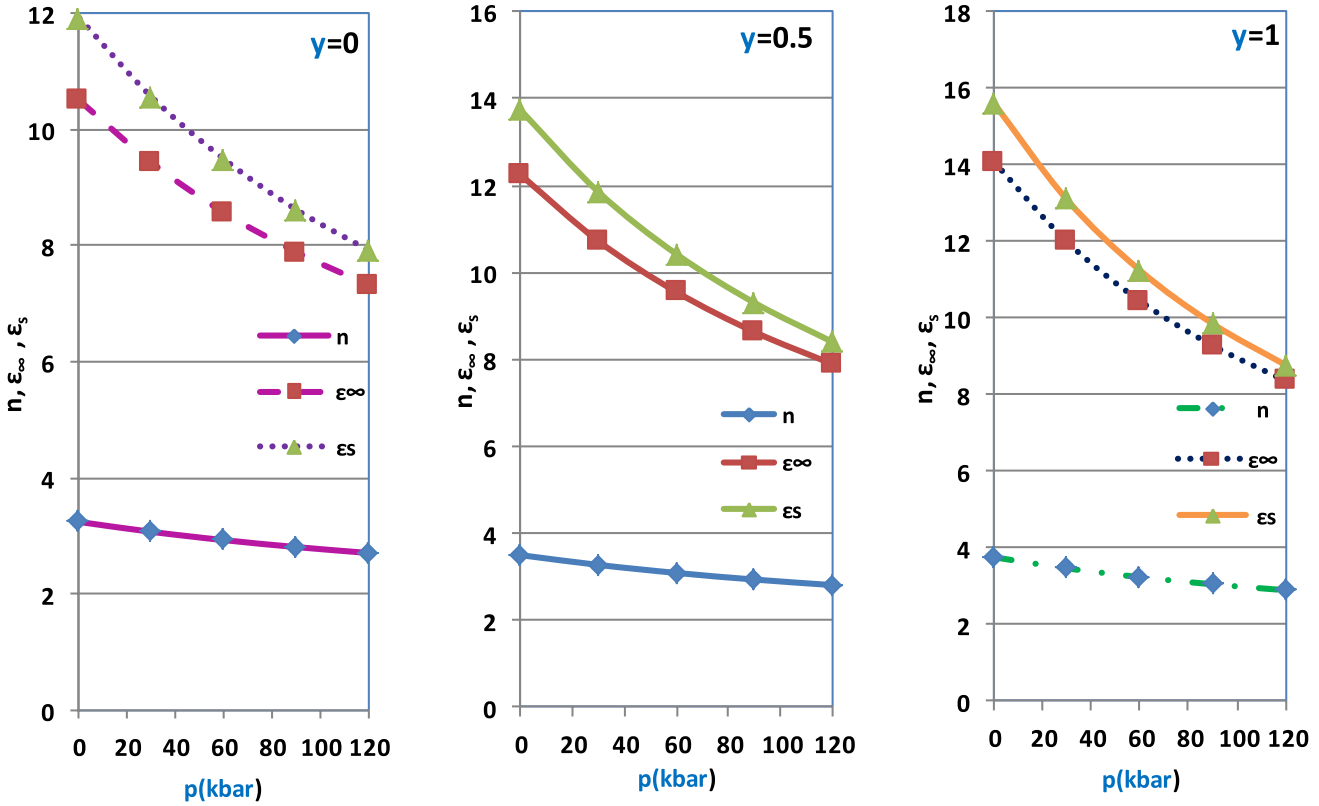

Fig. 5 The refractive index, optical dielectric constant and static dielectric constant of $InP_xAs_ySb_{1-x-y}$/InAs as function of pressure at constant values of compositional parameter y (0, 0.5, 1)

Table 5 The phonon frequencies ω_{LO} and ω_{TO} (10^{13} s^{-1}) of $InP_xAs_ySb_{1-x-y}$/InAs for different compositional alloys under the effect of pressure

P(kbar)	$y=0$		$y=0.5$		$y=1$	
	ω_{LO}	ω_{TO}	ω_{LO}	ω_{TO}	ω_{LO}	ω_{TO}
0	5.623	5.2788	4.9591	4.6825	4.4597, 4.5[a], 5.2[b]	4.2362, 4.1[a], 4.9[b]
30	6.1213	5.7837	5.5044	5.2342	5.0594	4.8423
60	6.635	6.308	6.0786	5.8192	5.7084	5.5026
90	7.1715	6.8585	6.6947	6.4499	6.4307	6.2405
120	7.74	7.444	7.3707	7.1438	7.2628	7.0915

[a]Ref. [43], [b]Ref. [45]

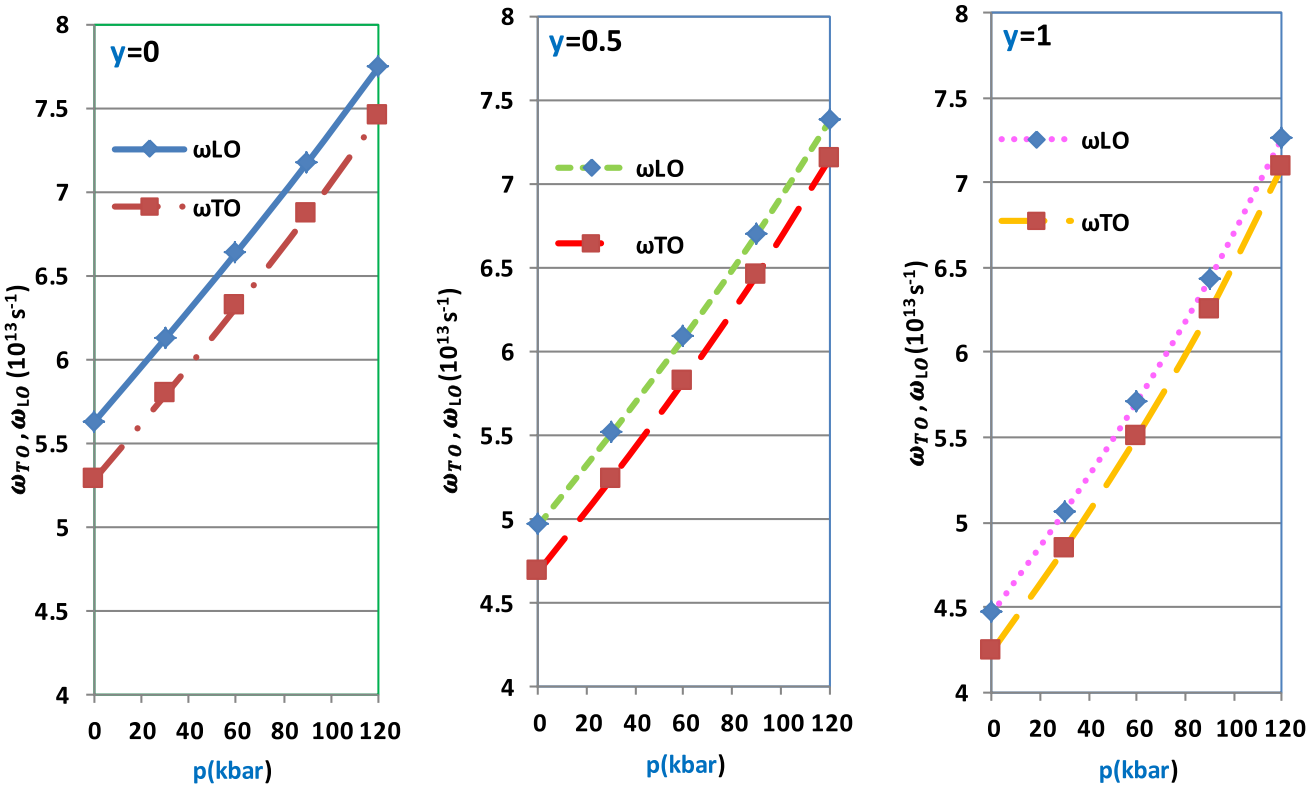

Fig. 6 The phonon frequencies ω_{LO} and ω_{TO} of $InP_xAs_ySb_{1-x-y}$/InAs as function of pressure at constant values of y-composition parameter (0, 0.5, 1)

5. References

1. M. Bosi, C. Pelosi, Prog. Photovolt. Res. Appl. **15**, 51 (2007)
2. J. Bowers, C. Burrus, J. Light. Technol. **5**, 1339 (1987)
3. C. Liu, Y. Li, Y. Zeng, Engineering **2**, 617 (2010)
4. E. A. Gutierrez-D, J. Deen, and C. Claeys, eds. *Low temperature electronics: physics, devices, circuits, and applications*. Elsevier, (2000)
5. R. J. Malik, ed. *III-V Semiconductor Materials and devices*. Elsevier (2012)
6. A.R. Degheidy, E.B. Elkenany, Mater. Chem. Phys. **143**, 1 (2013)
7. P. Malar, Ternary and Quaternary Semiconducting Compounds Thin Film Solar Cells. In *Thin Film Structures in Energy Applications*, Springer Cham, 85 (2015)
8. A.R. Degheidy, E.B. Elkenany, Thin Solid Films **539**, 365 (2013)
9. S. Adachi, III-V ternary and quaternary compounds. In *Springer handbook of electronic and photonic materials*, Springer, Cham, 1 (2017)
10. S. Adachi, J. Appl. Phys. **61**, 4869 (1987)
11. S. Adachi, *Properties of semiconductor alloys: group-IV, III-V and II-VI semiconductors*. John Wiley & Sons, **28**, (2009).
12. H. Mani, E. Tournie, J.L. Lazzari, C. Alibert, A. Joullie, B. Lambert, J. Cryst. Growth **121**, 463 (1992)
13. D. Chen, N.M. Ravindra, J Mater Sci **47**, 5735 (2012)
14. L.-C. Chen, W.-J. Ho, M.-C. Wu, Jpn. J. Appl. Phys **38**, 1314 (1999)
15. C. A. Wang, In *AIP Conference Proceedings*, American Institute of Physics, 255 (2004)
16. A.R. Degheidy, E.B. Elkenany, O.A. Alfrnwani, Silicon **9**, 183 (2017)
17. H. R. Jappor, M. A. Abdulsattar, and A. M. Abdul-Lettif. Electronic structure of AlP under pressure using semiempirical method. *Open Condens. Matter Phys. J.* **3**(1) (2010)
18. A.R. Degheidy, E.B. Elkenany, Chin. Phys. B **26**, 86103 (2017)
19. S. Saib, N. Bouarissa, P. Rodríguez-Hernández, A. Muñoz, Phys. B Condens. Matter **403**, 4059 (2008)
20. A.R. Degheidy, E.B. Elkenany, Semiconductors **45**, 1251 (2011)
21. A.R. Degheidy, A.M. Elabsy, H.G. Abdelwahed, E.B. Elkenany, Indian J. Phys. **86**, 363 (2012)
22. H. Y. Wang, J. Cao, X. Y. Huang, J. M. Huang, ArXiv Prepr ArXiv12046102 (2012)
23. E.B. Elkenany, Spectrochim. Acta Part A Mol. Biomol. Spectrosc. **150**, 15 (2015)
24. A.R. Degheidy, E.B. Elkenany, O. Alfrnwani, Comput. Condens. Matter **15**, 55 (2018)
25. N. Tiwari, A. Nirmal, M.R. Kulkarni, R.A. John, N. Mathews, Inorg. Chem. Front **7**, 1822 (2020)
26. J. Singh, V.K. Sharma, V. Kanchana, G. Vaitheeswaran, D. Errandonea, Mater. Today Commun. **26**, 101801 (2021)
27. J. Zagorac, D. Jovanović, T. Volkov-Husović, B. Matović, D. Zagorac, Model Simul. Mater. Sci. Eng. **28**, 35004 (2020)
28. M. Amrani, S. Ghemid, H. Meradji, S. Benayache, Y. Megdoud, R. Ahmad, R. Khenata, Comput. Condens. Matter **25**, e00514 (2020)
29. E. B. Elkenany, Energy band structure, acoustic velocities, optical phonon frequencies and mechanical properties of InP1-xSbx alloys under temperature and pressure. *Infrared Phys. Technol.*, **115**, 103720 (2021)
30. K.C. Pandey, J.C. Phillips, Phys. Rev. B **9**, 1552 (1974)
31. J.C. Phillips, K.C. Pandey, Phys. Rev. Lett. **30**, 787 (1973)
32. J.R. Chelikowsky, M.L. Cohen, Phys. Rev. B **14**, 556 (1976)

33. S.J. Lee, T.S. Kwon, K. Nahm, C.K. Kim, J. Phys. Condens. Matter **2**, 3253 (1990)
34. N. Bouarissa, H. Aourag, Phys. Stat. Solid **190**, 227 (1995)
35. P. Harrison. *Quantum wells, wires, and dots*. Chichester, UK: Wiley, (2016).
36. B. K. Ridley, *Quantum processes in semiconductors*. Oxford university press (2013)
37. R. Martin, Electronic Structure–Basic Theory and Practical Methods, Cambridge Univ. Pr., West Nyack, NY (2004)
38. P. Vogl, J. Phys. C Solid State Phys. **11**, 251 (1978)
39. S.-G. Shen, J. Phys. Condens. Matter **6**, 8733 (1994)
40. N. Bouarissa, Mater. Sci. Eng. B **100**, 280 (2003)
41. J.P. Walter, M.L. Cohen, Phys. Rev. **183**, 763 (1969)
42. J.P. Walter, M.L. Cohen, Phys. Rev. B **2**, 1821 (1970)
43. C. Kittel, P. McEuen, *Introduction to Solid State Physics* (Wiley, New York, 1976).
44. N. Bouarissa, Phys. B Condens. Matter **406**, 2583 (2011)
45. M. Boucenna, N. Bouarissa, F. Mezrag, Infrared Phys. Technol. **67**, 318 (2014)
46. H. Algarni, O.A. Al-Hagan, N. Bouarissa, T.F. Alhuwaymel, M.A. Khan, Philos. Mag. **98**, 2582 (2018)
47. N. Bouarissa, M. Boucenna, Phys. Scr. **79**, 15701 (2008)
48. S.F. Pugh, Lond. Edinb. Dublin Philos. Mag. J. Sci. **45**, 823 (1954)
49. S. Adachi, *Properties of group-iv, iii-v and ii-vi semiconductors*, vol. 16, John Wiley & Sons (2005)
50. M. S. Shur, *Handbook series on semiconductor parameters*, vol. 1, World Scientific (1996)
51. N. Bouarissa, Mater. Sci. Eng. B **86**, 53 (2001)
52. A.R. Degheidy, E.B. Elkenany, M.A.K. Madkour, A.M. AbuAli, Comput. Condens. Matter **16**, e00308 (2018)